ACS NANO

ARTICLE

DNA Self-Switchable Microlaser

Yifan Zhang, Xuerui Gong, Zhiyi Yuan, Wenjie Wang, and Yu-Cheng Chen*

Read Online

ACCESS | 📊 Metrics & More | 📖 Article Recommendations | 🔘 Supporting Information

ABSTRACT: Advances in switchable microlasers have emerged as a building block with immense potential in controlling light–matter interactions and integrated photonics. Compared to artificially designed interfaces, a stimuli-responsive biointerface enables a higher level of functionalities and versatile ways of tailoring optical responses at the nanoscale. However, switching laser emission with biological recognition has yet to be addressed, particularly with reversibility and wavelength tunability over a broad spectral range. Here we demonstrate a self-switchable laser exploiting the biointerface between label-free DNA molecules and dye-doped liquid crystal matrix in a Fabry–Perot microcavity. Laser emission switching among different wavelengths was achieved by utilizing DNA conformation changes as the switching power, which alters the orientation of the liquid crystals. Our findings demonstrate that different concentrations of single-stranded DNA lead to different temporal switching of lasing wavelengths and intensities. The lasing wavelength could be reverted upon binding with the complementary sequence through DNA hybridization process. Both experimental and theoretical studies revealed that absorption strength is the key mechanism accounting for the laser shifting behavior. This study represents a milestone in achieving a biologically controlled laser, shedding light on the development of programmable photonic devices at the sub-nanoscale by exploiting the complexity and self-recognition of biomolecules.

KEYWORDS: DNA, switchable biointerface, tunable microlaser, liquid crystals, microcavity
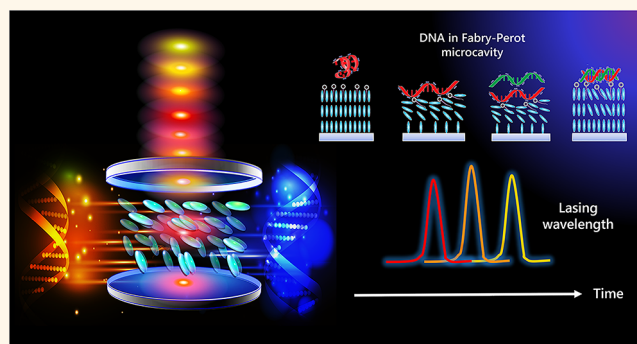
INTRODUCTION

Switchable interfaces have offered tremendous opportunities over the past decade, including bioelectronics,[1–4] optical devices,[3,5,6] laser switches,[7–10] biomedical sensors,[11,12] and fundamental biology.[13–15] In particular, the concept of "switchable biointerfaces" can be referred to as interfaces that change their microscopic properties in response to biological stimuli or biomolecular interactions. Contrary to artificially designed interfaces, switchable biointerfaces that take advantage of a biological system and biorecognition have demonstrated high functionality far beyond that obtained from nanomaterials.[16–18] Among all biomolecules, DNA is one of the most potent biomaterials known for its controllable synthesis and specificity of base-pair interactions.[19–21] Besides biomedical applications, the programmability and self-assembly of DNA structures offer versatile ways to construct DNA biointerfaces and tailor optical responses.[22–26] The stimuli-responsive properties of DNA molecules thus enable the development of program-switchable DNA interfaces.[16,25]

Recent developments in switchable DNA interfaces have been widely explored in controlling light–matter interactions, such as using fluorescently labeled DNA origami as modular adaptors to control light-emitting sites and inten-sities.[2,3,22–24,27] One peculiar application is to incorporate DNA with resonant structures to amplify its signal.[8,20,26,28,29] In this frame, liquid crystals (LC) can be envisaged as the ideal material for switching applications owing to their high responsivity to electrostatic interactions upon DNA binding events.[30–33] Recently, a few groups have shown that the binding activities of oligonucleotides (DNA) in the LC interfacial layer could induce significant reorientation at the aqueous interface.[32–35] That includes DNA hybridization, Watson–Crick base-pairing, and electrostatic interactions with proteins or drugs. Light will be modulated by the induced changes of refractive index or molecular orientation within the LC matrix.[36,37] As such, reflected light emissions or fluorescence emissions could be switched upon stimuli-response interactions at the biointerface by exploiting such features. Nonetheless, small footprints in DNA conformation

A
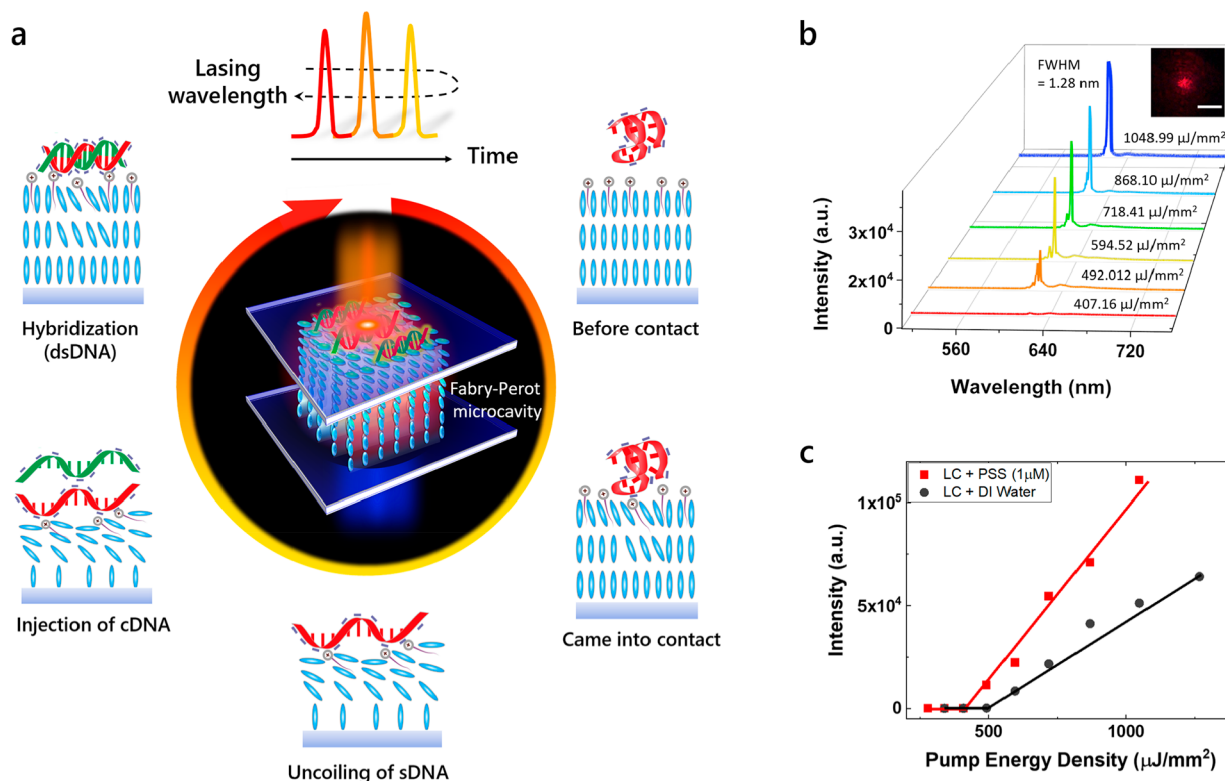
Figure 1. (a) Transitions of liquid crystal (LC) orientation during DNA hybridization. The center figure shows the optical setup of a LC matrix sandwiched in a Fabry−Perot microcavity. LC matrix orientations change from homeotropic to planar when ssDNA comes into contact with the LCs. The orientations are recovered to homeotropic after DNA hybridization. (b) Lasing spectra of liquid crystal matrix interacting with PSS solution under various pump energy densities. The inset shows a CCD image of the laser mode when above threshold. Scale bar represents 10 μm. (c) Comparison of the lasing threshold when DCM doped LC matrix interacted with PSS (1 μM) and water. Cavity size for all experiments was fixed at 150 μm. Excitation wavelength = 470 nm.

changes are often difficult to identify through conventional approaches.

In this study, we demonstrate a self-switchable laser by exploiting the interface between label-free oligonucleotides and dye-doped LC matrix in a Fabry−Perot (F−P) microcavity, in which the DNA interactions provide the switching power. Taking advantage of self-recognition of DNA and reconfigurability of liquid crystals (LC), laser emissions could be modulated by DNA conformation changes at the biointerface. The strong light−matter interaction induced by the microcavity thus enables subtle changes to be amplified within the cavity or liquid crystals.[37−45] As shown in Figure 1a, LCs change from homeotropic to planar alignment when single-stranded DNA (ssDNA) is adsorbed on the cationic monolayer of the matrix. The orientation changes of LC molecules thus resulted in a blue shift of lasing wavelength with pronounced signal amplification. DNA hybridization occurs upon the binding of complementary DNA targets to the single-stranded probes, which switches back the LC alignment, as well as lasing wavelengths, toward its initial state. Our results revealed that temporal shifting of lasing wavelength could be triggered by ssDNA concentration as low as 1 nM (approximately 9.6×10^8 bound targets per cm^2 area). Different concentrations of ssDNA lead to different temporal switching of lasing wavelength and lasing intensities in real-time. The kinetic fingerprints were unfolded for single- and double-stranded DNA, enabling high accuracy identification of the molecular binding affinities. The results may provide inspiration for the rational design of switchable lasers with performances based on the characteristic of organic and biological optoelectronic materials.

RESULTS AND DISCUSSION

Lasing Characteristics of PSS-Loaded Liquid Crystal Microlaser. We begin with the formation of the switchable microlaser by introducing liquid crystals inside a F−P microcavity formed by highly reflective dielectric mirrors. The experimental setup is provided in Supporting Information Figure S1. The orientations of liquid crystals are driven by the long-chain surfactant molecules (octadecyltrimethylammonium bromide, OTAB), in which OTAB is exploited to attract anionic molecules through electrostatic interactions. Assuming that all the OTAB molecules were adsorbed at the LC interface, the average surfactant is approximately four times more than the close-packed molecular area (0.83 molecule/nm^2). A monolayer of OTAB molecules was formed between the LC and water due to its amphiphilic nature. The alignment of LC matrixes, therefore, changes upon the binding of polyanionic molecules to the OTAB monolayer. As a proof-of-concept, we first investigated the lasing behavior by using poly(sodium 4-styrenesulfonate) (PSS) molecules as an analog to the DNA molecule for its polyanionic chain structure and the hydrophobic moieties. Herein PSS was first selected as the target molecule to stimulate the birefringence changes of LC matrixes. The polyanion PSS molecules were absorbed on the LC surface by electrostatic interactions with the OTAB cationic headgroups. As a control group, lasing was tested with an unperturbed LC cavity by inserting pure water.
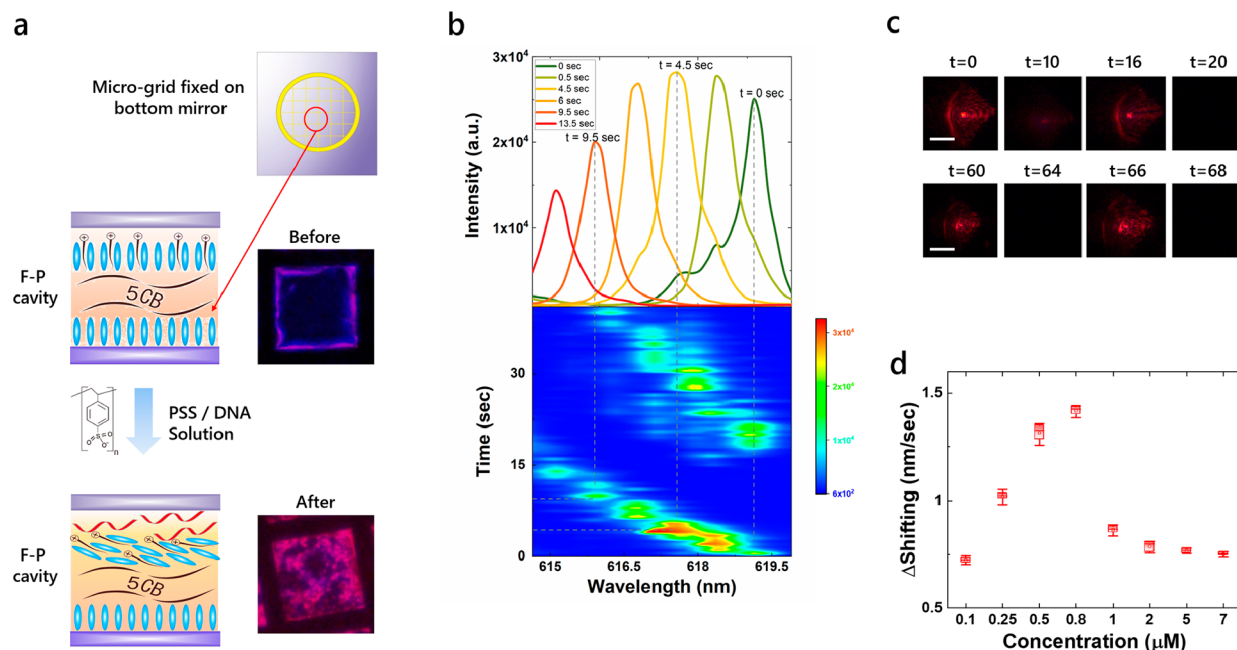
Figure 2. (a) Schematic of the LC matrix filled in microgrids. The right panel shows the polarized optical microscopic image before and after PSS sample injection. Dark state indicates that liquid crystals are in homeotropic alignment. Bright state reveals the change of liquid crystal alignment. The photos show a grid length of 200 μm. (b) Lasing spectrum of the LC matrix after infiltration of 1 μM PSS solution. The top image indicates the blue-shifting behavior of the lasing peak. The bottom image shows the periodic shifting behavior of laser emissions. (c) Lasing modes captured by CCD at different time periods with switching behavior. Scale bars represent 10 μm for all photos. (d) Summary of lasing wavelength shifting rates under different PSS concentrations. For each concentration, the error bars and statistics were based on three individual measurements. Cavity size, 150 μm. Excitation wavelength = 470 nm.

Without LC interactions, a broad lasing spectrum with multiple modes was observed (Supporting Information Figure S2a). After PSS molecules infiltrated into the cavity, a narrow lasing spectrum emerged, as shown in Supporting Information Figure S2b. The full width half-maximum (fwhm) is about 1.28 nm. However, the F−P cavity gave rise to a significantly lower lasing threshold when filled with PSS molecules than that with pure water. The lasing spectra under various pump energy densities are provided in Figure 1b. The threshold difference presented in Figure 1c is mainly due to the LC cell orientations as a consequence of dye absorption. Since the maximum absorption occurs when the incident light is linearly polarized along the molecular axis, the homeotropically aligned LC cell possesses a higher threshold than that in planar alignment.[33,34,46] Note that the overall fwhm and threshold of lasing emissions are relatively large. Due to the huge cavity length between the two mirrors, additional loss and misalignment may be induced in the cavity. However, both issues could be improved if a smaller spacer and smaller volume of LC matrix were fabricated.

Figure 2a explicitly presents the change of the DCM-doped LC device before and after interaction with PSS molecules under an optical microscope. Before addition of PSS solution, the grid appears uniformly dark, demonstrating that LC cells remained in a homeotropic alignment. When PSS comes in contact with LC matrixes, the hydrophobic interaction between the PSS side groups and liquid crystals promotes the intercalation of the polymer chain into the LC matrix. After PSS adsorption, the grid turned bright, indicating that the alignment of liquid crystals is in the same direction as the analyzer. Such changes of the liquid crystal orientation were also verified under the polarized optical microscope in Supporting Information Figure S3. (The mechanism of liquid crystal orientation is provided in Supporting Information). Figure 2b further presents the dynamic lasing profile after the infiltration of PSS solution into the F−P cavity, where the top panel shows the spectral output of the lasing emission. The bottom panel of Figure 2b shows the temporal profiles of the lasing emission, where the lasing peak wavelengths and intensities vary accordingly. Figure 2c confirmed such a phenomenon with CCD images, where the lasing modes act as a flashlight switching back and forth in numerous cycles. The lasing hot spot first appears in the center, then slowly decays and reappears again.

To further explore the lasing characteristics after PSS adsorption, different concentrations of PSS solution (0.1, 0.25, 0.5, 0.8, 1 μM) were injected into individual LC cells, respectively. To our surprise, the results show that the switching rate of laser mode varies with PSS concentrations. When the PSS concentration increases, temporal switching of the laser modes increased accordingly, as shown in Figure 2d. Higher PSS concentrations resulted in larger tilted angles and birefringence, hence generating a larger switching rate. However, the switching rate reaches its maximum when the PSS concentration approaches 0.8 μM (Figure 2d). Further loading of PSS molecules will increase the surface viscosity and thus cannot reflect additional disturbance (Supporting Information Figure S4).

Laser Switching upon ssDNA Interaction. Next, we employed single-stranded DNA (ssDNA) as the target analyte to study its laser switching behavior. It is noteworthy that ssDNA has a similar structure as PSS in terms of a polyanion and hydrophobic side groups. Additionally, its physical properties could be altered by hybridization to its complementary bases, which provides an ideal platform to revert the switching of lasing wavelength. The schematic concept of
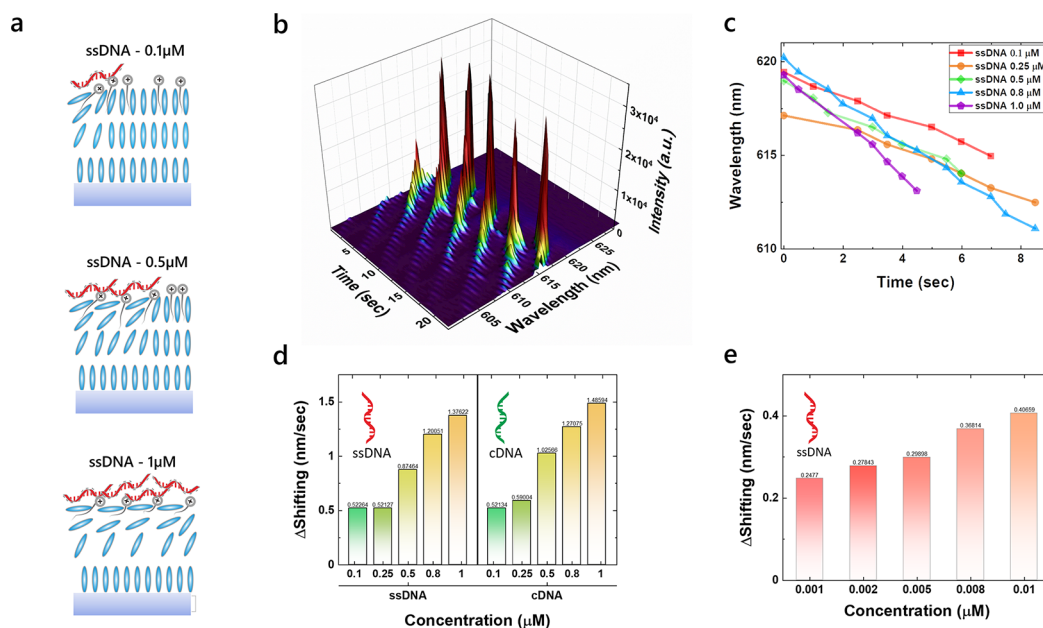
Figure 3. (a) Illustration of the ssDNA surface coverage with increasing concentrations. At the biointerface, the LCs change their homeotropic orientation and affect the bulk alignment of the LC matrix. (b) Three-dimensional plot of the lasing spectrum when 1 μM ssDNA solution was applied to the LC cell. The shifting of the lasing spectrum is periodic. (c) Time trajectories of lasing peak wavelengths (blue shift) when LC interacted with different ssDNA concentrations (0.1, 0.25, 0.5, 0.8, and 1 μM). (d) (left) Summary of the wavelength shifting rate under different ssDNA concentrations extracted from panel c. (right) Summary of the wavelength shifting rate under different cDNA concentrations. Five different concentrations were applied (0.1, 0.25, 0.5, 0.8, and 1 μM). (e) Summary of the wavelength shifting rate at extremely low ssDNA concentrations. All data were averaged from 3 individual measurements. Cavity size of 150 μm. Excitation wavelength = 470 nm.
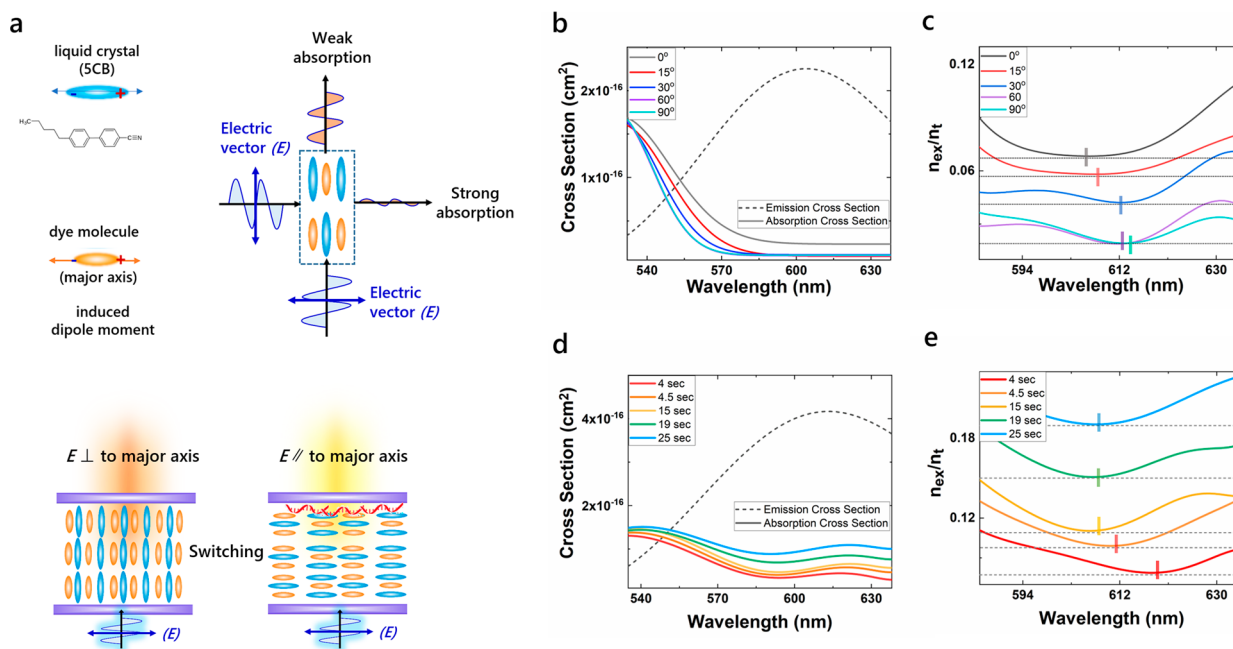
Figure 4. (a) Interaction between liquid crystal molecules (5CB) and DCM dye molecules. Weak absorption occurs when the electric vector (E) of incident light is perpendicular to the major axis of the dye molecule; strong absorption occurs when the electric vector (E) of incident light is parallel to the major axis of the dye molecule. The bottom panel shows the switching of DCM−LC orientation when ssDNA molecules are added in a F−P cavity. (b) Absorption cross sections measured from DCM−LC under different incident light polarization. (c) Fraction of DCM molecules in the excited state required at lasing threshold based on different absorption cross sections in panel b. (d) Absorption cross sections measured at different times after applying ssDNA molecules in the DCM−LC matrix. (e) Fraction of DCM molecules in the excited state required at lasing threshold based on different absorption cross sections in panel d after applying ssDNA. Note that the emission cross section of DCM (dashed curves) and effective refractive index of LC ($n = 1.6$) were fixed for the calculations in panels c and e.

applying ssDNA for laser switching is shown in Figure 3a. A similar laser switching phenomenon was obtained when ssDNA interacts with the biointerface of LC matrixes, as presented in Figure 3b. The appearance of the lasing peaks blue shifts periodically with a gradually decreasing lasing intensity. However, the shifting behavior reaches a dynamic equilibrium after several cycles when LC molecules become stable in the cavity. By application of different ssDNA concentrations (0.1, 0.25, 0.5, 0.8, 1 μM), the laser mode trajectories between 620 and 612 nm were extracted and plotted in Figure 3c. In particular, the trajectories of laser modes showed a linear relationship through time, while the offsets remained similar at each concentration. The left panel of Figure 3d summarizes the laser switching rate under different ssDNA concentrations. The increase of ssDNA molecules at the LC interface resulted in larger ssDNA surface coverage and stronger LC−ssDNA interactions. As such, more liquid crystals will transform into planar alignment at a faster pace, thus changing the laser modes. Note that a similar trend was also found by exploring its complementary single-stranded DNA (cDNA) under different concentrations (the right panel of Figure 3d). The findings here demonstrate that any sequence of ssDNA possesses the ability to trigger such laser switching. To demonstrate that the proposed laser is not limited to a specific dye, LC matrix was doped with green emission dye to show similar lasing capability (Supporting Information Figure S5).

Lastly, in Figure 3e, we accessed the threshold limit of ssDNA concentration by analyzing the switching rate at lower concentrations. As the disturbance at lower concentration is gentler, the detectable ssDNA motion depends on the surface coverage of ssDNA molecules and the induced liquid crystal zenithal tilt. Figure 3e plots the average switching per second for ssDNA at 0.01 μM, 0.008 μM, 0.005 μM, 0.002 μM, and 0.001 μM. The average switching rate becomes very small when the concentration approaches 1 nM. Eventually, the minimum concentration to obtain laser switching is approximately 1 nM, which is about 9.6×10^8 nucleotides per cm^2 area.

Mechanism of Laser Switching Behavior. To elucidate the underlying mechanism of laser switching behavior, different lasing threshold conditions caused by the optical properties of DCM and LC matrix were evaluated. When PSS or ssDNA molecules interact with LC matrix, the orientation of liquid crystal molecules (5CB) will also cause a significant impact on the surrounding dye molecule orientations. Previous studies have mentioned that doping dyes into liquid crystals creates a guest−host complex, in which the permanent dipole moment of LC molecules generates an induced dipole moment on the dye molecules (Figure 4a).[47,48] The alignment of dye molecules will thus change with the directional change of liquid crystal mesogens. Herein, the DCM dye molecules align their major axes according to LC molecule orientation in the matrix, resulting in possible changes of optical density, absorption, and emission intensity. In particular, our findings demonstrated that absorption strength plays a dominant role in laser switching, as depicted in Figure 4a. When the major axis of the dye molecule is parallel to the electric vector (E) of incident light, there is strong absorption. In contrast, when the major axis is perpendicular to the electric vector of incident light, only weak absorption exists. The bottom panel of Figure 4a illustrates the orientation changes of DCM dye-doped liquid

crystal (DCM−LC) matrix when ssDNA molecules are added in a F−P cavity.

To demonstrate that the absorption strength of the DCM molecule is highly polarization-dependent on incident light, we altered the polarization of the excitation beam and measured its absorption. As illustrated in Figure 4b, the absorption cross-section of DCM−LC matrix was measured by tuning the incident polarization from 90° to 0°, which corresponds to an electric vector (E) perpendicular and parallel to the major axis of DCM molecule. Apparently, the absorption becomes larger as the incident polarization changed from 90° to 0°. By adopting a laser rate equation model, the fraction of excited DCM molecules can be expressed by n_{ex}/n_t, where n_t is the total concentration of DCM and n_{ex} is the concentration of DCM in the excited state. Details for the theoretical calculation can be found in the Supporting Information. As such, the required population inversion (n_{ex}/n_t) corresponding to different polarization was derived (Figure 4c). From Figure 4c, we can clearly see that the lasing wavelength blue shifted as the polarization changed from 90° to 0°. It is also noteworthy that the required lasing threshold (n_{ex}/n_t) increased as the lasing peak blue shifted. This indicates that the lasing intensity should decrease as the lasing blue shifts under a fixed pump energy density. Both above-mentioned phenomena agree well with our experimental results and assumption.

On this basis, next, we experimentally measured the absorption cross-section of DCM−LC matrix when it interacted with ssDNA molecules. Figure 4d presents the absorption cross-section of the DCM−LC matrix obtained at different times after addition of ssDNA molecules. When ssDNA interacts with LC molecules, the LC will alter the orientation of the DCM dye molecules, resulting in different absorption cross sections through time. Here we can clearly observe that the absorption gradually increases through time. Considering the Q-factor and dye concentration used, we calculated the required population inversion in Figure 4e based on the absorption cross sections in Figure 4d. The dashed lines in Figure 4e represents the minimum required lasing threshold (n_{ex}/n_t) corresponding to the respective time (and absorption strength). To our surprise, a significant blue shift of lasing wavelength was observed. Consequently, the required lasing threshold increased as the lasing peak blue shifts, which is consistent with our observation in Figure 3.

Besides the contribution of DCM dye absorption, we also investigated the impact of effective refractive indices and fluorescence emission intensity in Supporting Information Figure S6. The Q-factor of F−P cavity should be consistent during the sample infiltration since the cavity was carefully fixed with a magnetic spacer. While the cavity length and the polarization of pump are fixed throughout the experiment, the reorientation of the liquid crystals gives rise to change of the effective refractive indices. Again, we used the rate equation to study the lasing output by considering $n = 1.52-1.71$ in the DCM−LC matrix (corresponding to ordinary and externally refractive indices). After performing the theoretical calculation in Supporting Information Figure S6a,b, we concluded that the rise of the medium effective indices of liquid crystals only changes the lasing threshold (and intensity). It has negligible effect on the lasing wavelength shift.

Lastly, we considered the fluctuation of the DCM fluorescence emission intensity when ssDNA interacted with the DCM−LC matrix. The emission intensity was measured at different times and converted into emission cross sections in
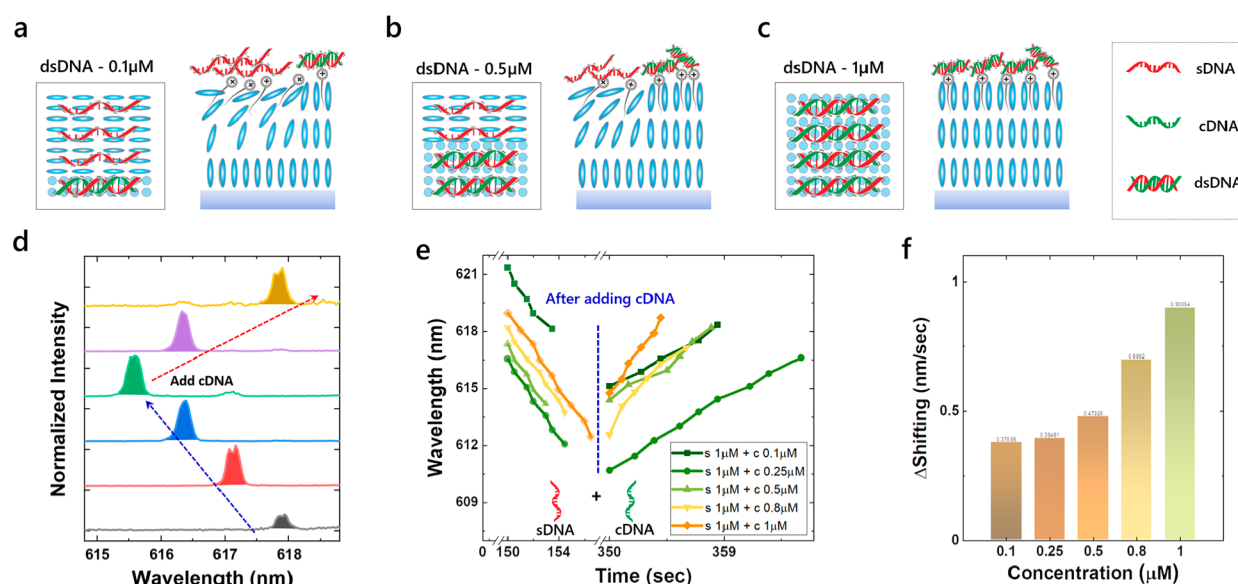
Figure 5. (a–c) Illustration of the interfacial interactions between DNAs and liquid crystals. A fixed concentration of ssDNA was adhered to the interface where different concentrations of cDNA were applied. LC matrix tends to form planar alignment in the ssDNA region and homeotropic alignment in dsDNA regions. (d) Laser switching before and after adding cDNA onto ssDNA-probed LC matrix. The shifting direction reverts upon DNA hybridization. (e) Time trajectories of lasing peak wavelengths of ssDNA-probed LC cells before (blue shift) and after (red shift) adding cDNA solutions. Five different concentrations of cDNA (0.1, 0.25, 0.5, 0.8, and 1 μM) were applied to ssDNA-probed LC matrix (1 μM). (f) Summary of the wavelength shifting rate extracted from panel e after adding different cDNA concentrations. All data in panel f were averaged from 3 individual measurements. Cavity size of 150 μm. Excitation wavelength = 470 nm.

Supporting Information Figure S6c. By adoption of the rate equation model, the required population inversion was derived and plotted in Supporting Information Figure S6d. Similar to refractive indices, only lasing thresholds will be affected; however, no shifting behavior was found. In summary, our findings demonstrate that absorption is the key mechanism that determines the laser shifting behavior. In contrast, the fluctuations of effective refractive indices and fluorescence emission intensity will only lead to the changes of lasing threshold (and intensity).

Laser Switching upon DNA Hybridization. One of the most interesting properties of liquid crystals is that the LC reorients from homeotropic to planar upon ssDNA adsorption and reverts upon DNA hybridization when the ssDNA binds to its complementary partner. The hybridization process folds the hydrophobic base pairs of single-strand DNA inside the double helix, which leads to more efficient packing. Since DNA hybridization can revert the liquid crystal orientation, we hypothesized that the lasing switching rate could be modulated by DNA hybridization in real-time. To investigate the impact of hybridization on lasing behavior, we prepared LC samples coated with 1 μM ssDNA as a probe and injected different concentrations of cDNA (0.1, 0.25, 0.5, 0.8, 1 μM). The concept is illustrated in Figure 5a–c, where the nucleation of the homeotropic domain (Figure 4a) will grow and coalesce as the cDNA concentration increases. By fixing the amount of ssDNA on the LC interface, more dsDNA pairs will be formed when a higher concentration of cDNA is applied. As a proof-of-concept, Figure 5d clearly shows that before adding cDNA (only ssDNA), the lasing peak blue shifts through time. When cDNA binds to ssDNA, the specific binding causes the lasing peak to red shift toward its initial wavelength. The same phenomena were discovered for all cDNA concentrations applied, where Figure 5e shows the red-shifting behavior after different cDNA concentrations bind to ssDNA. Before binding

to cDNA, one can observe that the average switching rate for pure ssDNA (1 μM) is about 1.0 nm/s (blue-shifting); however, the rates begin to differentiate after binding the different concentrations of cDNA (during DNA hybridization). As shown in Supporting Information Figure S7, the appearance of the lasing peaks red shifts periodically with a gradually increasing lasing intensity. However, the shifting behavior reaches a dynamic equilibrium after several cycles. This may be the result of photobleaching and hence fewer gain molecules can be stimulated. Overall, we summarized the average switching rate of ssDNA before and after binding with respective cDNA concentrations (0.1, 0.25, 0.5, 0.8, 1 μM) in Figure 5f. The switching rate was found to be proportional to the binding cDNA concentrations.

As a control group, we prepared five ssDNA (1 μM) samples and mixed them with 0.1, 0.25, 0.5, 0.8, and 1 μM cDNA in individual tubes. The samples were preannealed before the lasing experiments. Thus, we could have a mixture equivalent to 0.1 μM dsDNA, 0.25 μM dsDNA, 0.5 μM dsDNA, 0.8 μM dsDNA, and 1 μM dsDNA, respectively. Then we infiltrated the preannealed dsDNA samples into the LC cells. Since the intercalation of DNA strands in the LC matrix plays an essential role in the switching process, an opposite trend was found in Supporting Information Figure S8 as compared to Figure 4f. Since preannealed dsDNA cannot intercalate into the LC matrix without hydrophobic interaction, the highest preannealed dsDNA concentration (or lowest ssDNA) produced the lowest switching rate, whereas in Figure 5f, ssDNA was first intercalated into the LC matrix before hybridization, folding the hydrophobic moieties inside the resulting dsDNA. Consequently, the highest switching rate occurred at the highest hybridized dsDNA concentration.

CONCLUSION

In this study, we introduced the concept of a switchable biolaser by taking advantage of the organic biomolecule DNA hybridization process. By exploitation of the electrostatic forces between ssDNA and surface-modified LC matrix, the structural changes of unlabeled DNA trigger the azimuthal rotation of liquid crystals, resulting in laser mode switching. Our findings revealed that different ssDNA concentrations cause average temporal switch at a different rates, which are proportional to the ssDNA concentration. Interestingly, the laser switching process could be reverted by binding with its complementary partner (cDNA) through the DNA hybridization process.

The significance of this study is to introduce the concept of using organic biomolecules to switch coherent light sources at different wavelengths. By exploiting the complexity and self-recognition of DNA sequences, laser light could be fully manipulated and programmed. The ability for specific molecular recognition could be potentially suitable for applications such as information encoding and data storage with laser light in the future. On the other hand, stimuli-responsive biointerfaces have played an essential role in light−matter interactions and integrated photonics. We believe this work represents a milestone in achieving biological-controlled laser, offering critical insights for switchable devices that take advantage of the self-recognition or self-regulation of biomolecules to modulate light at the sub-nanoscale.

Finally, we would like to point out that the hybridization process could also be implemented in molecular detection. We admit that the current settings are not sensitive enough for ideal sensing applications (~1 nM). As mentioned, the current cavity length (spacer) is exceptionally large. The sensitivity could be significantly improved if a smaller spacer is used in the future. The thinner the DCM−LC matrix (smaller volume), the lower amount of ssDNA molecules are required to trigger the switching of laser emissions (surface to volume ratio will increase significantly).

MATERIALS AND METHODS

Preparation of Microcavity and Liquid Crystal Cells. The F−P microcavity was formed by two customized dielectric mirrors with high reflectivity from 550 to 650 nm. The bottom mirror was cleaned by immersing it in a mixture of DI water, reagent alcohol, and KOH in the ratio of 1:5:1. Then the mirror was immersed in a mixture of toluene and trichloro(octyl)silane (OTS) (in the ratio of 10:0.003 at 50 °C. After 1 h, the mirror was rinsed first with toluene, followed by acetone, ethanol, and DI water, and dried in nitrogen. Before introducing the liquid crystals into the cavity, we examined the contact angle of the OTS-coated mirror under a microscope to ensure that the mirror surface was sufficiently hydrophobic to promote homeotropic alignment of liquid crystals. We then used the mirrors for the preparation of liquid crystal cells.

The mixture of nematic liquid crystal (4′-pentyl-4-biphenylcarbonitrile, 5CB, Tokyo Chemicals), 0.3 wt % laser dye (4-(dicyanomethylene)-2-methyl-6-(4-dimethylaminostyryl)-4H-pyran, DCM), and 100 μM octadecyltrimethylammonium bromide (OTAB) was immersed in an ultrasonic bath for 15 min to form a homogeneous liquid crystal solution. Then a piece of copper TEM grid was placed on the OTS-treated mirror. After that, 1.5 μL of liquid crystal solution was dripped onto the grid. The excess liquid crystal solution was removed using a 20 μL capillary tube. After that, 150 μm spacers were placed near the edges of the bottom mirror. Finally, the cell was covered with the top mirror. All chemicals were purchased from Sigma-Aldrich unless specified.

Preparation of DNA Materials. The DNA sequences used were 16-mer ssDNA, 5′-AGAAAAAACTTCGTGC-3′, and 16-mer cDNA,

5′-TCTTTTTTTGAAGCACG-3′, both purchased from Sigma-Aldrich. For experiments without annealing (either ssDNA or cDNA only), the ssDNA was injected directly into the microcavity to interact with the LC matrixes. For hybridization (with annealing) experiments, five tubes of 1 μM ssDNA and 1 tube each of 0.1, 0.25, 0.5, 0.8, and 1 μM cDNA solution were first prepared. Then the ssDNA was mixed with the respective cDNA solution in the tube. The five tubes were placed in a 95 °C hot bath. After 2 min, they were taken out and cooled to 25 °C. All the dsDNA samples were ready for use after 45 min and subsequently injected into the microcavity.

Optical Measurements and Setup. The bright field polarized optical images were taken with a Nikon-E200 polarized microscope. For all the lasing measurements, an inverted microscopic system (Nikon Ti2) with 20×, 0.4 NA objective was used to excite the microcavity and collect laser emission. A pulsed nanosecond-laser (EKSPLA PS8001DR) integrated with an optical parametric oscillator was used to achieve optical pump (repetition rate 50 Hz; pulse duration 5 ns). The excitation wavelength set for DCM was 470 nm. The pump energy density was adjustable by a continuously variable neutral density filter. The pumping beam diameter at the objective focal plane was ~16 μm wide. The emission light was collected through the same objective, then separated by a beam splitter, and sent into a charge-coupled device camera and imaging spectrometer (Andor Kymera 328i and Newton 970 EMCCD), as plotted in Figure S1.

ASSOCIATED CONTENT

ⓢ Supporting Information

The Supporting Information is available free of charge at https://pubs.acs.org/doi/10.1021/acsnano.0c08219.

> Schematic diagram of the optical experiment setup, lasing comparison between water and PSS solution, polarization of LC grid changing after injection of ssDNA solution, the appearance of the LC grid with different amounts of surfactant, switching lasing with coumarin 6-doped LC matrix, the effect of refractive indices and emission fluctuations, red shift behavior of lasing wavelength after infiltration of cDNA in ssDNA chip (DNA hybridization), summary of the average lasing wavelength shift for preannealed dsDNA, and calculation of required population inversion (PDF)

AUTHOR INFORMATION

Corresponding Authors

Wenjie Wang − *Key Lab of Advanced Transducers and Intelligent Control System of Ministry of Education, Taiyuan University of Technology, Taiyuan 030024, P. R. China*; Email: wangwenjie@tyut.edu.cn

Yu-Cheng Chen − *School of Electrical and Electronic Engineering and School of Chemical and Biomedical Engineering, Nanyang Technological University, 639798, Singapore*; ⓞ orcid.org/0000-0002-0008-5601; Email: yucchen@ntu.edu.sg

Authors

Yifan Zhang − *School of Electrical and Electronic Engineering, Nanyang Technological University, 639798, Singapore*

Xuerui Gong − *School of Electrical and Electronic Engineering, Nanyang Technological University, 639798, Singapore*

Zhiyi Yuan − *School of Electrical and Electronic Engineering, Nanyang Technological University, 639798, Singapore*

Complete contact information is available at:
https://pubs.acs.org/10.1021/acsnano.0c08219

Author Contributions

Y. Zhang and Y.-C. Chen designed the experiment and wrote the paper; Y. Zhang performed the liquid crystal and DNA experiments; Y. Zhang and X. Gong did the data analysis; Y. Zhang, Z. Yuan, and Y.-C. Chen conducted the theoretical analysis; W. Wang fabricated the mirrors.

Notes

The authors declare no competing financial interest.

REFERENCES

(1) Parlak, O.; Turner, A. P. Switchable Bioelectronics. *Biosens. Bioelectron.* **2016**, *76*, 251−265.

(2) Graugnard, E.; Kellis, D. L.; Bui, H.; Barnes, S.; Kuang, W.; Lee, J.; Hughes, W. L.; Knowlton, W. B.; Yurke, B. DNA-Controlled Excitonic Switches. *Nano Lett.* **2012**, *12*, 2117−2122.

(3) Back, S. H.; Park, J. H.; Cui, C.; Ahn, D. J. Bio-Recognitive Photonics of a DNA-Guided Organic Semiconductor. *Nat. Commun.* **2016**, *7* (1), 10234.

(4) Privman, M.; Tam, T. K.; Pita, M.; Katz, E. Switchable Electrode Controlled by Enzyme Logic Network System: Approaching Physiologically Regulated Bioelectronics. *J. Am. Chem. Soc.* **2009**, *131* (3), 1314−1321.

(5) Kuehne, A. J. C.; Gather, M. C.; Eydelnant, I. A.; Yun, S.-H.; Weitz, D. A.; Wheeler, A. R. A Switchable Digital Microfluidic Droplet Dye-Laser. *Lab Chip* **2011**, *11*, 3716−3719.

(6) Tang, S. K. Y.; Li, Z.; Abate, A. R.; Agresti, J. J.; Weitz, D. A.; Psaltis, D.; Whitesides, G. M. A Multi-Color Fast-Switching Microfluidic Droplet Dye Laser. *Lab Chip* **2009**, *9*, 2767−2771.

(7) Gao, Z.; Zhang, W.; Yan, Y.; Yi, J.; Dong, H.; Wang, K.; Yao, J.; Zhao, Y. S. Proton-Controlled Organic Microlaser Switch. *ACS Nano* **2018**, *12*, 5734−5740.

(8) Zhang, X.; Lee, W.; Fan, X. Bio-Switchable Optofluidic Lasers Based on DNA Holliday Junctions. *Lab Chip* **2012**, *12*, 3673−3675.

(9) Lv, Y.; Xiong, Z.; Yao, Z.; Yang, Y.; Xiang, S.; Zhang, Z.; Zhao, Y. S. Steric-Hindrance-Controlled Laser Switch Based on Pure Metal-Organic Framework Microcrystals. *J. Am. Chem. Soc.* **2019**, *141* (51), 19959−19963.

(10) Kim, D. S.; Lee, W.; Lopez-Leon, T.; Yoon, D. K. Self-Regulated Smectic Emulsion with Switchable Lasing Application. *Small* **2019**, *15* (49), 1903818.

(11) Zhang, Y.; Tang, Z.; Wang, J.; Wu, H.; Maham, A.; Lin, Y. Hairpin DNA Switch for Ultrasensitive Spectrophotometric Detection of DNA Hybridization Based on Gold Nanoparticles and Enzyme Signal Amplification. *Anal. Chem.* **2010**, *82*, 6440.

(12) Plaxco, K. W.; Soh, H. T. Switch-Based Biosensors: A New Approach towards Real-Time, *in Vivo* Molecular Detection. *Trends Biotechnol.* **2011**, *29* (1), 1−5.

(13) Zhang, Q.; Zhou, Z.; Li, C.; Wu, P.; Sun, M. pH-Switchable Coordinative Micelles for Enhancing Cellular Transfection of Biocompatible Polycations. *ACS Appl. Mater. Interfaces* **2019**, *11* (23), 20689−20698.

(14) Levskaya, A.; Weiner, O. D.; Lim, W. A.; Voigt, C. A. Spatiotemporal Control of Cell Signalling Using a Light-Switchable Protein Interaction. *Nature* **2009**, *461* (7266), 997−1001.

(15) Koçer, G.; ter Schiphorst, J.; Hendrikx, M.; Kassa, H. G.; Leclère, P.; Schenning, A. P.; Jonkheijm, P. Light-Responsive Hierarchically Structured Liquid Crystal Polymer Networks For Harnessing Cell Adhesion and Migration. *Adv. Mater.* **2017**, *29* (27), 1606407.

(16) Yin, F.; Mao, X.; Li, M.; Zuo, X. Stimuli-Responsive DNA-Switchable Biointerfaces. *Langmuir* **2018**, *34* (49), 15055−15068.

(17) Zhou, Y.; Zheng, Y.; Wei, T.; Qu, Y.; Wang, Y.; Zhan, W.; Zhang, Y.; Pan, G.; Li, D.; Yu, Q.; Chen, H. Multistimulus Responsive Biointerfaces with Switchable Bioadhesion and Surface Functions. *ACS Appl. Mater. Interfaces* **2020**, *12* (5), 5447−5455.

(18) Sun, A.; Lahann, J. Dynamically Switchable Biointerfaces. *Soft Matter* **2009**, *5* (8), 1555−1561.

(19) Behnia, S.; Fathizadeh, S.; Javanshour, E.; Nemati, F. Light-Driven Modulation of Electrical Current through DNA Sequences: Engineering of a Molecular Optical Switch. *J. Phys. Chem. B* **2020**, *124* (16), 3261−3270.

(20) Sun, Y.; Shopova, S. I.; Wu, C.-S.; Arnold, S.; Fan, X. Bioinspired Optofluidic FRET Lasers *via* DNA Scaffolds. *Proc. Natl. Acad. Sci. U. S. A.* **2010**, *107*, 16039−16042.

(21) Ren, X.; Xu, Q.-H. Label-Free DNA Sequence Detection with Enhanced Sensitivity and Selectivity Using Cationic Conjugated Polymers and PicoGreen. *Langmuir* **2009**, *25*, 43−47.

(22) Szukalski, A.; Moffa, M.; Camposeo, A.; Pisignano, D.; Mysliwiec, J. All-Optical Switching In Dye-Doped DNA Nanofibers. *J. Mater. Chem. C* **2019**, *7* (1), 170−176.

(23) Kuzyk, A.; Jungmann, R.; Acuna, G. P.; Liu, N. DNA Origami Route for Nanophotonics. *ACS Photonics* **2018**, *5* (4), 1151−1163.

(24) Lan, X.; Wang, Q. DNA-Programmed Self-Assembly of Photonic Nanoarchitectures. *NPG Asia Mater.* **2014**, *6* (4), e97−e97.

(25) Harroun, S. G.; Prévost-Tremblay, C.; Lauzon, D.; Desrosiers, A.; Wang, X.; Pedro, L.; Vallée-Bélisle, A. Programmable DNA Switches and their Applications. *Nanoscale* **2018**, *10* (10), 4607−4641.

(26) Gopinath, A.; Miyazono, E.; Faraon, A.; Rothemund, P. W. K. Engineering and Mapping Nanocavity Emission *via* Precision Placement of DNA Origami. *Nature* **2016**, *535* (7612), 401−405.

(27) Park, S. M.; Park, G.; Cha, Y. J.; Yoon, D. K. Generation of 2D DNA Microstructures *via* Topographic Control and Shearing. *Small* **2020**, *16*, 2002449.

(28) Chen, Q.; Liu, H.; Lee, W.; Sun, Y.; Zhu, D.; Pei, H.; Fan, C.; Fan, X. Self-Assembled DNA Tetrahedral Optofluidic Lasers with Precise and Tunable Gain Control. *Lab Chip* **2013**, *13*, 3351−3354.

(29) Lee, W.; Chen, Q.; Fan, X.; Yoon, D. K. Digital DNA Detection Based on a Compact Optofluidic Laser with Ultra-Low Sample Consumption. *Lab Chip* **2016**, *16* (24), 4770−4776.

(30) Verma, I.; Sidiq, S.; Pal, S. K. Poly (L-Lysine)-Coated Liquid Crystal Droplets For Sensitive Detection Of DNA and their Applications in Controlled Release of Drug Molecules. *ACS Omega* **2017**, *2* (11), 7936−7945.

(31) Humar, M. Liquid-Crystal-Droplet Optical Microcavities. *Liq. Cryst.* **2016**, *43* (13−15), 1937−1950.

(32) Lai, S. L.; Huang, S.; Bi, X.; Yang, K.-L. Optical Imaging of Surface-Immobilized Oligonucleotide Probes on DNA Microarrays Using Liquid Crystals. *Langmuir* **2009**, *25* (1), 311−316.

(33) Price, A. D.; Schwartz, D. K. DNA Hybridization-Induced Reorientation of Liquid Crystal Anchoring at the Nematic Liquid Crystal/Aqueous Interface. *J. Am. Chem. Soc.* **2008**, *130* (26), 8188−8194.

(34) McUmber, A. C.; Noonan, P. S.; Schwartz, D. K. Surfactant−DNA Interactions at the Liquid Crystal−Aqueous Interface. *Soft Matter* **2012**, *8* (16), 4335−4342.

(35) Lai, S. L.; Hartono, D.; Yang, K.-L. Self-Assembly of Cholesterol DNA at Liquid Crystal/Aqueous Interface and its Application For DNA Detection. *Appl. Phys. Lett.* **2009**, *95* (15), 153702.

(36) Xiang, J.; Varanytsia, A.; Minkowski, F.; Paterson, D. A.; Storey, J. M.; Imrie, C. T.; Lavrentovich, O. D.; Palffy-Muhoray, P. Electrically Tunable Laser Based on Oblique Heliconical Cholesteric Liquid Crystal. *Proc. Natl. Acad. Sci. U. S. A.* **2016**, *113* (46), 12925−12928.

(37) Zhang, Y.; Yuan, Z.; Qiao, Z.; Barshilia, D.; Wang, W.; Chang, G. E.; Chen, Y. C. Tunable Microlasers Modulated by Intracavity Spherical Confinement with Chiral Liquid Crystal. *Adv. Opt. Mater.* **2020**, *8*, 1902184.

(38) Chen, Y. C.; Fan, X. Biological Lasers for Biomedical Applications. *Adv. Opt. Mater.* **2019**, *7* (11), 1900377.

(39) Chen, Y.-C.; Tan, X.; Sun, Q.; Chen, Q.; Wang, W.; Fan, X. Laser-Emission Imaging of Nuclear Biomarkers for High-Contrast Cancer Screening and Immunodiagnosis. *Nat. Biomed. Eng.* **2017**, *1* (9), 724−735.

(40) Ignesti, E.; Tommasi, F.; Fini, L.; Martelli, F.; Azzali, N.; Cavalieri, S. A New Class of Optical Sensors: A Random Laser Based Device. *Sci. Rep.* **2016**, *6*, 35225.

(41) Rivera, J. A.; Eden, J. G. Flavin Mononucleotide Biomolecular Laser: Longitudinal Mode Structure, Polarization, And Temporal Characteristics as Probes of Local Chemical Environment. *Opt. Express* **2016**, *24* (10), 10858−10868.

(42) Nizamoglu, S.; Lee, K.-B.; Gather, M. C.; Kim, K. S.; Jeon, M.; Kim, S.; Humar, M.; Yun, S.-H. A Simple Approach to Biological Single-Cell Lasers *via* Intracellular Dyes. *Adv. Opt. Mater.* **2015**, *3*, 1197−1200.

(43) Gather, M. C.; Yun, S. H. Single-Cell Biological Lasers. *Nat. Photonics* **2011**, *5*, 406−410.

(44) Yuan, Z.; Wang, Z.; Guan, P.; Wu, X.; Chen, Y. C. Lasing-Encoded Microsensor Driven by Interfacial Cavity Resonance Energy Transfer. *Adv. Opt. Mater.* **2020**, *8* (7), 1901596.

(45) Humar, M.; Gather, M. C.; Yun, S.-H. Cellular Dye Lasers: Lasing Thresholds and Sensing In A Planar Resonator. *Opt. Express* **2015**, *23*, 27865−27879.

(46) Anni, M.; Lattante, S. *Organic Lasers: Fundamentals, Developments, and Applications*; Pan Stanford Publishing: Singapore, 2018.

(47) Sharma, V.; Kumar, P. Studies Of Absorption Coefficient Cum Electro-Optic Performance of Polymer Dispersed Liquid Crystal Doped with CNT and Dichroic Dye. *Phys. B* **2017**, *524*, 118−122.

(48) Sheng, M.; Zhang, L.; Wang, D.; Li, M.; Li, L.; West, J. L.; Fu, S. Fabrication Of Dye-Doped Liquid Crystal Microcapsules For Electro-Stimulated Responsive Smart Textiles. *Dyes Pigm.* **2018**, *158*, 1−11.